# Supplementary Information

# Boosting Bifunctional Oxygen Electrocatalysis of Graphitic $C_3N_4$ using Non-covalently Functionalized Non-oxidized Graphene Aerogels as Catalyst Supports

*Jin Kim,[b, 1] Anand P. Tiwari,[a, 1] Myungwoo Choi,[a] Qiang Chen,[a] Jinho Lee,[a] Travis G. Novak,[a] Minsu Park,[a] Kisun Kim,[a] Ki-Seok An[b, *] and Seokwoo Jeon[a,*]*

[a] Department of Materials Science and Engineering, Korea Advanced Institute of Science and Technology, Daejeon 34141, Republic of Korea
E-mail: jeon39@kaist.ac.kr

[b]Thin Film Materials Research Center, Korea Research Institute of Chemical Technology, Daejeon 34114, Republic of Korea
E-mail: ksan@krict.re.kr

[1]These authors contributed equally to this work

*corresponding author, E-mail address: *jeon39@kaist.ac.kr* (S. Jeon), *ksan@krict.re.kr*

(K.-S. An)

**CONTENTS**

**Experimental Section**

**Fabrication of g-$C_3N_4$ Nanosheets:** Melamine (100 mg) was heated at 550 $^oC$ for 4 hours in air with elevating temperature of 5 $^oC$ $min^{-1}$. The resulting bulk g-$C_3N_4$ was immersed in De-ionized (DI) water (100 ml) and exfoliated using a probe sonicator for 2 hours. The g-$C_3N_4$ solution was centrifuged at 1500 rpm for 30 min and the supernatant was collected.

**Fabrication of NOGFs:** Bulk potassium metal and naphthalene were dissolved in anhydrous tetrahydrofuran (THF) in 1 M concentration to prepare potassium-naphthalenide solution. Graphite powder (Sigma Aldrich) was immersed in the potassium-naphthalenide solution for at least 24 hr to obtain graphite intercalation compound (GIC). The GIC was thoroughly washed with anhydrous THF to remove remaining potassium and naphthalene. The GIC ultra-sonicated using a probe sonicator in Dimethyl for 30 minutes. For obtaining surface modified NOGFs, the GIC was immersed in PVP-Dimethyl Sulfoxide (2 mg $ml^{-1}$) or PBA-Dimethyl Sulfoxide (2 mg $ml^{-1}$) solution. The exfoliated NOGF solution was then centrifuged at 1500 rpm for 30 min and the supernatant was collected.

**Fabrication of Aerogel:** NOGFs and g-$C_3N_4$ nanosheets were first redispersed in DI water in 1:1 ratio and redispersed in DI water in 4 mg $ml^{-1}$ concentration under probe sonication for 3 min. Nafion binder was sequentially added to the solution at 1:4 weight ratio of NOGFs and g-$C_3N_4$ nanosheets. The precursor solution was then poured into a polylactic acid (PLA) mold with one end having 20$^o$ wedge. The mold was placed on a metal stage cooled by liquid nitrogen for bi-directional freeze casting. The aerogel was obtained after freeze dried in a freeze dryer (TFD8501, iSBio) for 48 hr.

**Characterization:** SEM (S-4800, Hitachi) with a field-emission source at 10 keV and built-in EDS was used to examine the structure and composition of CN-NOGAs. TEM analysis was performed with F2 F20 (Tecnai) at an acceleration voltage of 200 keV. Raman spectroscopy was carried out on a Senterra system (Bruker). XPS was performed on a Sigma Probe system (Thermo VG Scientific) with AlKα radiation source. XRD (D/MAX-2500) with Cu Kα radiation (λ = 1.518 Å) was used to examine phases and composition of Cn-NOGAs. Fourier transform infrared (FT-IR) spectroscopy was carried out by FT-IR-4100 type-A FT-IR

spectrometer (Jasco). Hall measurement was performed with Ecopia. For accurate comparison, the CN-NOGAs were formed into films with the same dimension by compressing to 5 µm thickness and cut into 5 cm x 5 cm. The films were placed above the film holder and measured.

**Electrochemical Characterizations:** The aerogels were cut with a punch hole with diameter of 3 mm, in the direction parallel to the pore alignment direction. The samples were placed on top of glassy carbon electrode. 5 µl of Nafion 117 solution (5%) was drop casted on the sample which was dried in an oven at 65 °C overnight. The electrocatalytic properties were measured on a VersaSTATE 3 (principle applied research) electrochemical workstation equipped with a rotating disk electrode system (AMETEK, principle applied research, 616B). The electrochemical performance was evaluated using a three-electrode system (where the working electrode was the active material/glassy carbon, the reference electrode was Ag/AgCl in 3 M KCl, and the counter electrode was a Pt mesh) in 1 M KOH (pH = 13.6) electrolyte. All of the potentials were calibrated to a RHE, ERHE = EAg/AgCl + 0.196 + 0.0591 pH V.

**Details for calculating the Koutecky-Levich plots:**

The Koutecky - Levich plots and the kinetic parameters of ORR can be analysed on the basis of the Koutecky - Levich equations:

$$\frac{1}{j} = \frac{1}{j_L} + \frac{1}{j_K} = \frac{1}{B\omega^{\frac{1}{2}}} + \frac{1}{j_K} \quad (1)$$

$$B = 0.62nFC_0\left(D_0^{\frac{2}{3}}\right)\eta^{-\frac{1}{6}} \quad (2)$$

$$j_K = nF\ kC_0 \quad (3)$$

Where j (mA $cm^{-2}$) is the measured current density, $j_K$ and $j_L$ (mA $cm^{-2}$) are the kinetic- and diffusion-limiting current densities, ω is the angular velocity of the rotating disk (ω = 2πN, N is the linear rotating speed in rpm), n is the overall number of electrons transferred in ORR, F is the Faraday constant, $C_0$ is the bulk concentration of $O_2$, $D_0$ is diffusion coefficient of $O_2$, ν is the kinematic viscosity of the electrolyte, and k is the electron transfer rate constant, respectively. According to the Equations (1) and (2), the number of electrons transferred (n) and the kinetic-limiting current $j_K$ can be obtained from the slope and intercept of the Koutecky–Levich plots (1/j versus $\omega^{-1/2}$). For the calculation of electron transfer number n and $j_K$ in 0.1M KOH electrolyte, values of different constants are estimated as:

F= Faraday constant = 96485 C $mol^{-1}$

A= electrode area = 0.071 $cm^2$

$D_0$ = Diffusion coefficient of $O_2$ $= 9 \times 10^{-5}$

ν = kinematic viscosity of the electrolyte solution = 0.01 $cm^2\ s^{-1}$

$C_0$ = concentration of dissolved $O_2$ $= 1.2 \times 10^{-6}$

After putting these values in equation (2) we got the final equation as:

$$n = \frac{28.15}{slope\ \ of\ \ K-L\ \ plot} \quad (4)$$

Furthermore, for the calculation of the production yield of $H_2O_2$, we have used the following equation:

$$H_2O_2\,\% = 100 \times \frac{4 - n}{2} \quad (5)$$

**Values for the samples:**

| Samples | Electron transfer number ($n_e$) | Kinetic current density ($j_k$) |
|---|---|---|
| g-$C_3N_4$ | 0.10 | 0.15 mA $cm^{-2}$ |
| CN-NOGA | 0.35 | 0.31 mA $cm^{-2}$ |
| p-type CN-NOGA | 0.65 | 1.62 mA $cm^{-2}$ |
| n-type CN-NOGA | 3.80 | 5.20 mA $cm^{-2}$ |
| Pt/C | 3.99 | 5.90 mA $cm^{-2}$ |

**Details for calculating the $n_e$ based on rotating ring disc electrode (RRDE) measurements:**

$n_e$ of the n-type CN-NOGA was calculated on the basis of the RRDE measurements using the following equation:

$$n_e = 4I_D/(I_D + I_R/N) \qquad (6)$$

Where N (= 0.36) is the collection efficiency, $I_D$ is the faradic disk current, and $I_R$ is the faradic ring current.

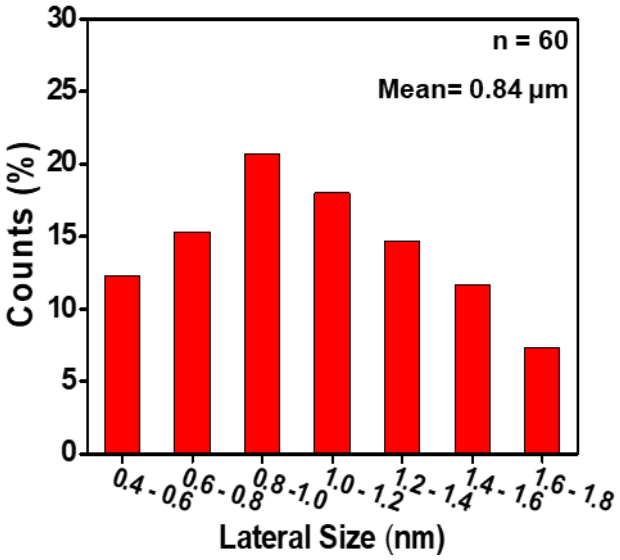


**Fig. S1.** Lateral size distribution of 60 g-$C_3N_4$ nanosheets.

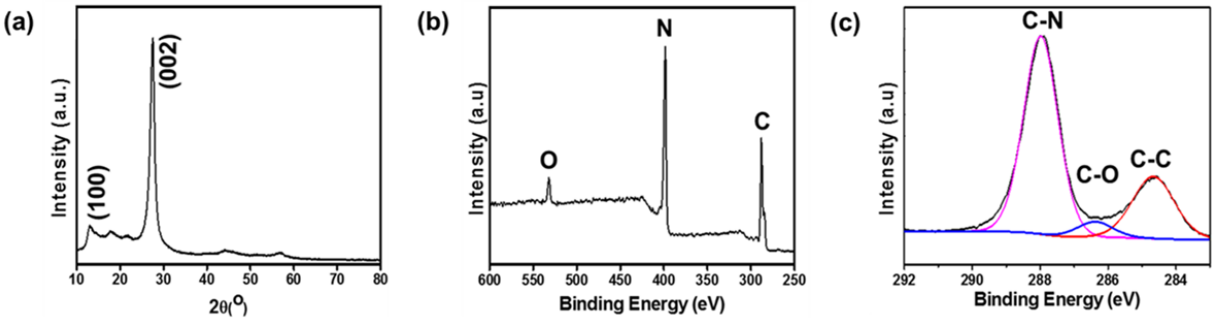


**Fig. S2.** Characterization of the exfoliated g-$C_3N_4$ nanosheets. (a) X-ray diffraction pattern (XRD) showing characteristic peaks of g-$C_3N_4$. X-ray photoelectron spectroscopy (XPS) analysis of g-$C_3N_4$ nanosheets in (b) survey and (c) C1s peak showing characteristic 60 % nitrogen and C-N content.

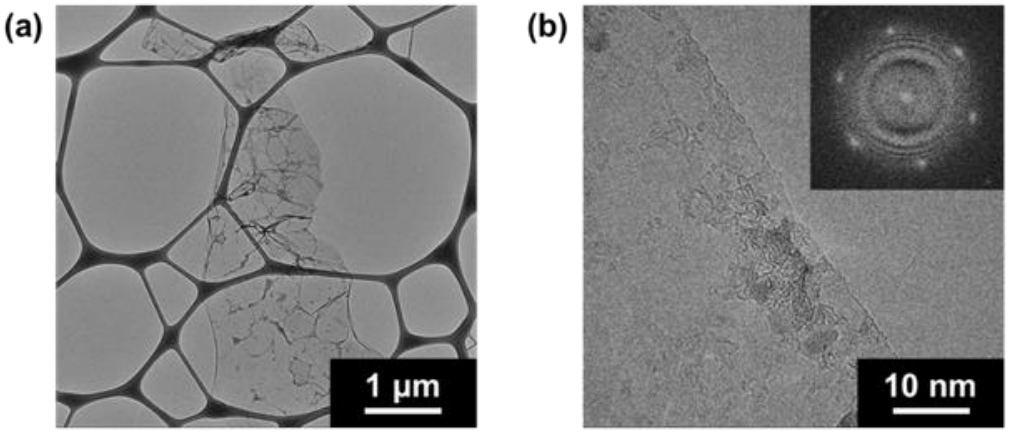


**Fig. S3**. Characterization of the non-oxidized graphene flake (NOGF). (a) Transmission electron microscopy (TEM) image of a single NOGF and (b) enlargement of its edge (inset shows Fast Fourier Transform (FFT) pattern of hexagonal symmetry, indicating of high crystallinity).

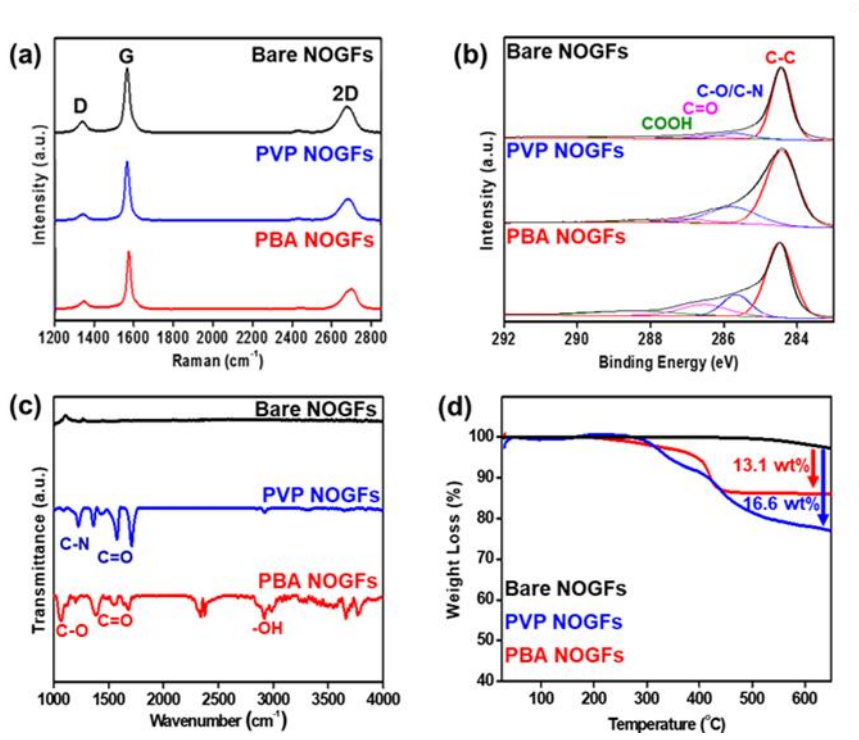


**Fig. S4.** Composition analysis of NOGFs with different surface modifications. (a) Raman spectrum showing low $I_D/I_G$ ratios of NOGFs even after surface modification with PVP or PBA. (b) XPS C1s peaks and (c) Fourier Transform Infrared Spectroscopic (FT-IR) analysis showing characteristic components of corresponding surfactant. (d) Thermogravimetric analysis (TGA) estimating the quality of functionalized surfactant.

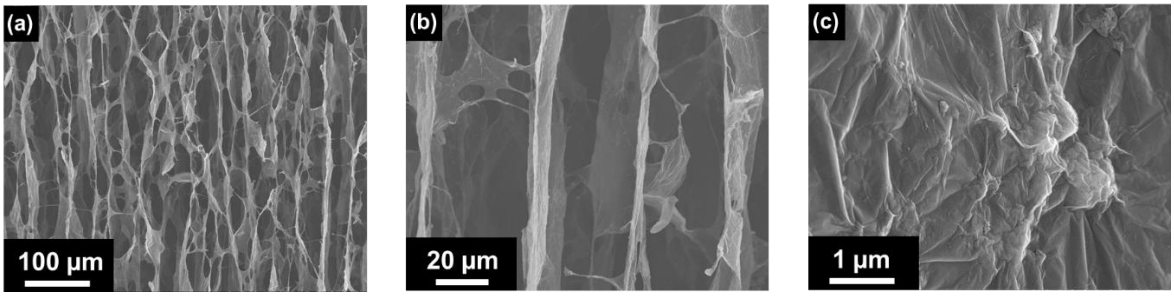


**Fig. S5.** Magnified SEM image of n-type CN-NOGA pore walls.

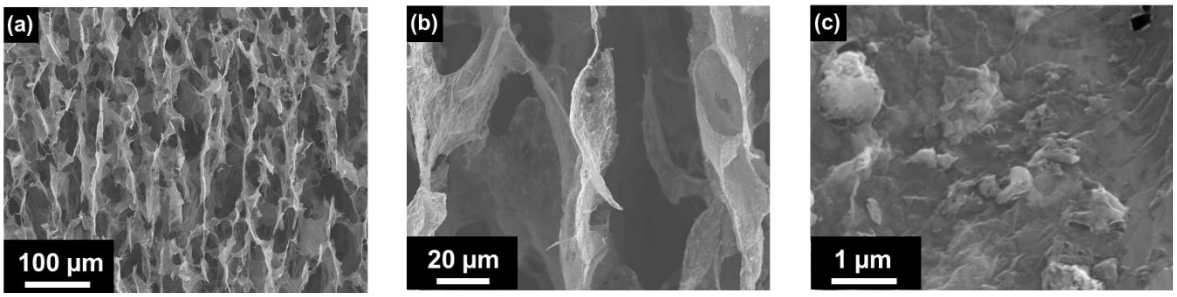


**Fig. S6.** Magnified SEM image of p-type CN-NOGA pore walls.

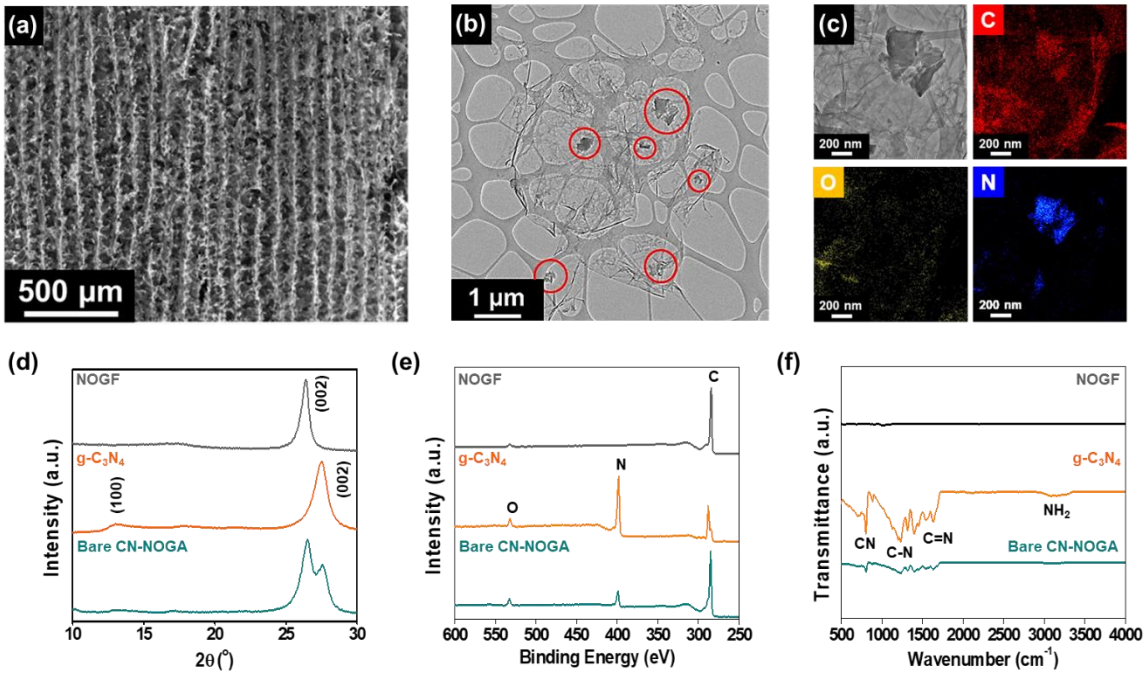


**Fig. S7.** (a) SEM image of the cross section of bare CN-NOGA. (b) TEM image of bare CN-NOGA pore wall and corresponding (c) energy-dispersive X-ray spectroscopy (EDS) elemental maps of C, O and N. Characterization of bare NOGF, g-$C_3N_4$ and bare CN-NOGA in (d) X-ray Diffraction (XRD), (e) X-ray photoelectron spectroscopy (XPS) survey and (f) Fourier transform infrared (FT-IR) spectroscopy.

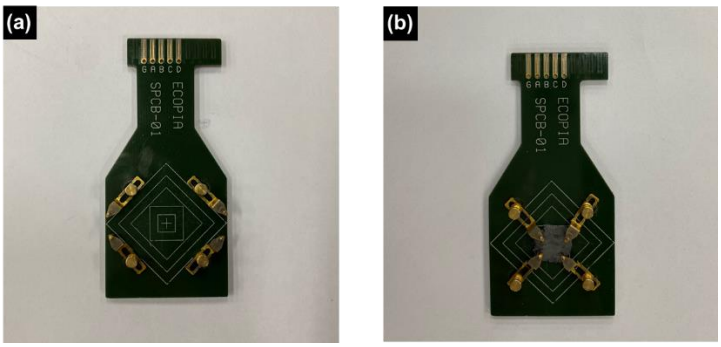


**Fig. S8.** Digital image of (a) film holder for Hall measurement. (b) Film holder with CN-NOGA in 5 cm x 5 cm and 5 μm thickness dimension.

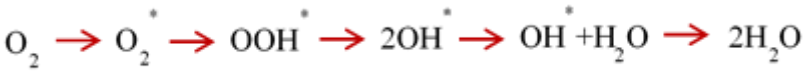


**Fig. S9.** Ideal oxygen reduction reaction through four electron donation.

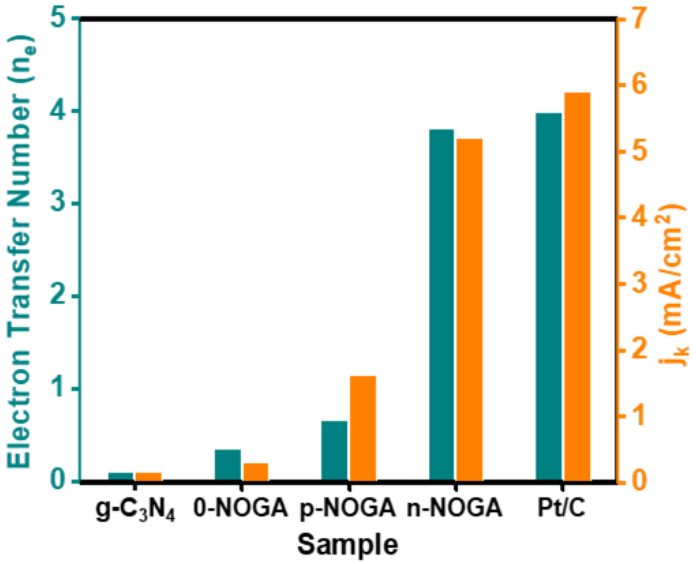


**Fig. S10.** Electron transfer number ($n_e$) and kinetic current density ($j_k$) of bare g-$C_3N_4$, CN-NOGAs in different electric states and commercial Pt/C.

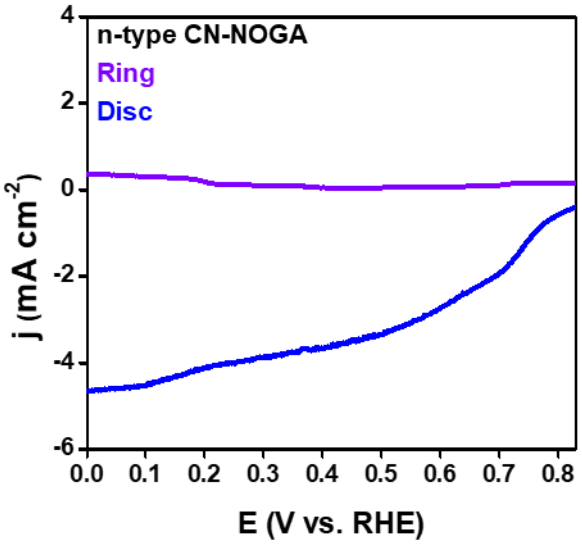


**Fig. S11.** RRDE polarization curves of n-type CN-NOGA in 1.0 M KOH at a rotation rate of 1600 rpm.

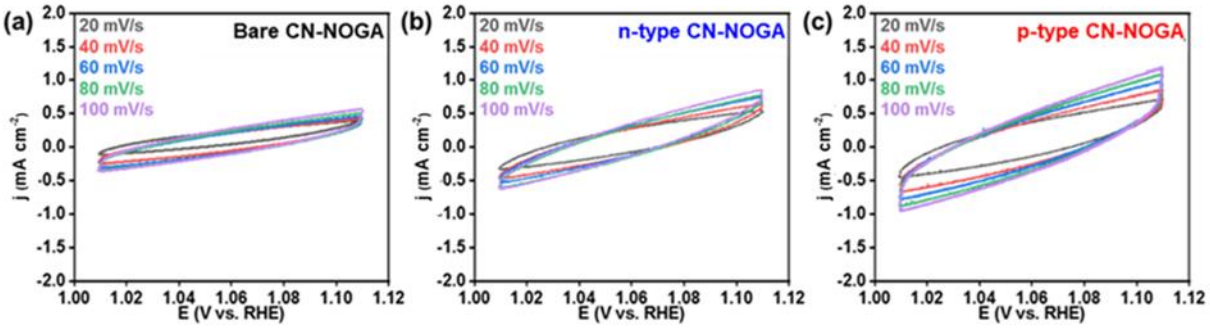


**Fig. S12.** Cyclic voltammetry of (a) bare CN-NOGA, (b) n-type CN-NOGA and (c) p-type CN-NOGA.

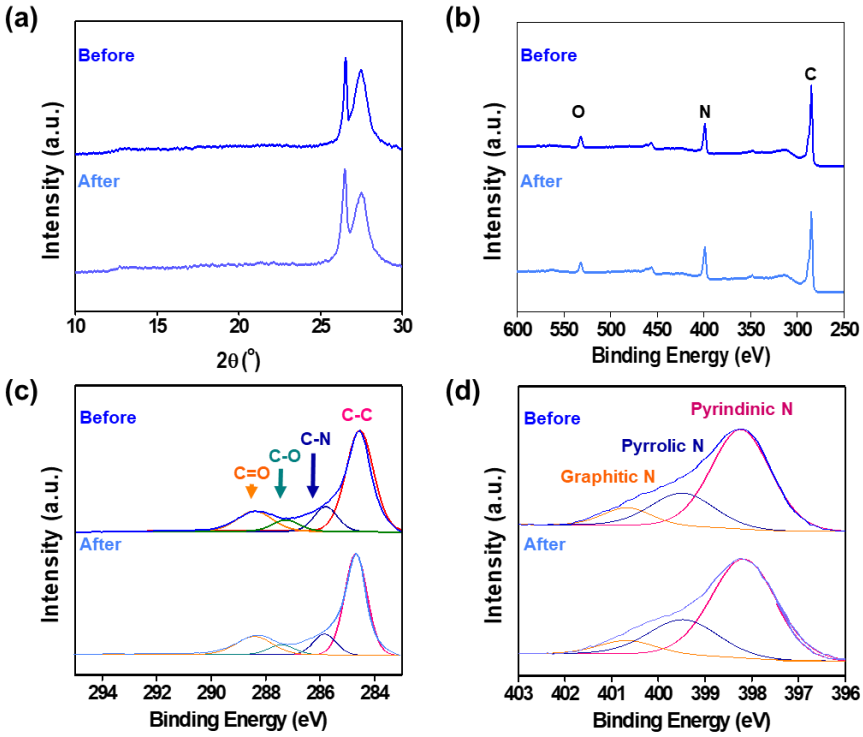


**Fig. S13.** Composition analysis of n-type CN-NOGA before and after ORR stability test: (a) XRD spectra, XPS in terms of (b) survey, (c) C1s peaks and (d) N1s peaks.

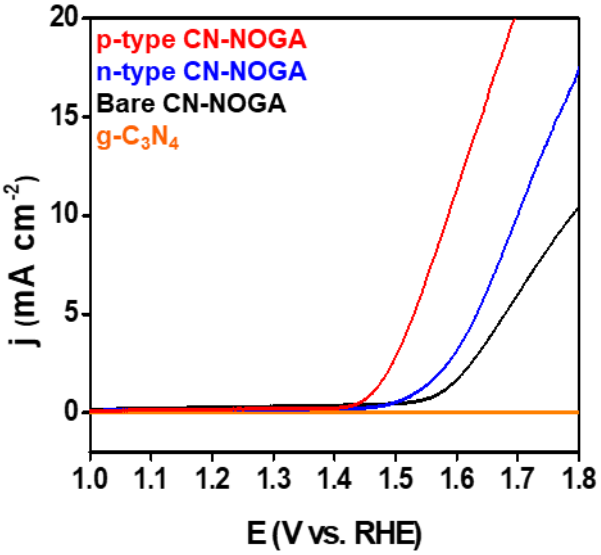


**Fig. S14.** Linear sweep voltammetry curves of as-prepared g-$C_3N_4$ and CN-NOGAs normalized by ECSAs.

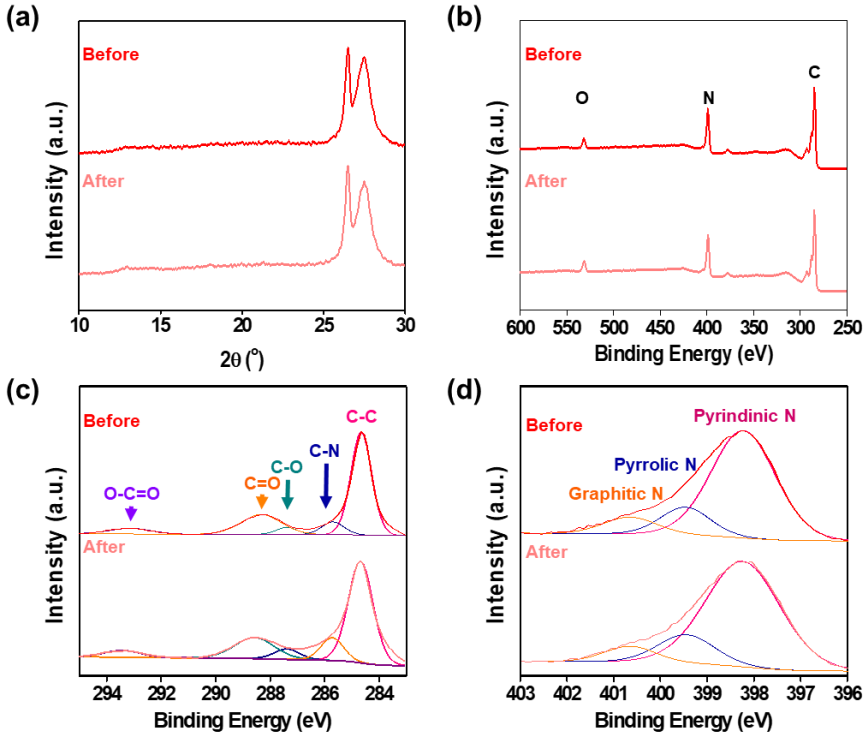


**Fig. S15.** Composition analysis of p-type CN-NOGA before and after OER stability test: (a) XRD spectra, XPS in terms of (b) survey, (c) C1s peaks and (d) N1s peaks.

**Table S1.** Hall measurement of NOGFs in different surface modifications.

| | Carrier Concentration ($cm^{-3}$) | Mobility ($cm^2 \cdot V^{-1} \cdot s^{-1}$) | Resistivity ($\Omega \cdot cm$) | Conduction Type |
|---|---|---|---|---|
| 0 CN-NOGA (Bare) | $0.588 \cdot 10^{19}$ | $1.451 \cdot 10^{2}$ | $7.31 \cdot 10^{-3}$ | n |
| n CN-NOGA (PVP) | $4.114 \cdot 10^{19}$ | $1.238 \cdot 10^{2}$ | $1.23 \cdot 10^{-3}$ | n |
| p CN-NOGA (PBA) | $1.348 \cdot 10^{19}$ | $1.202 \cdot 10^{2}$ | $3.85 \cdot 10^{-3}$ | p |

**Table S2.** Comparison of present work with other reported bifunctional oxygen electrocatalysis based on g-$C_3N_4$ supported on various conductive supports. All shown V0 values are vs. RHE.

| **Sample** | **Overpotentials ($V_0$ *vs* RHE) for ORR/electron transfer no. ($n_e$)** | **Overpotential of OER ($V_0$ *vs* RHE) @10 mA $cm^{-2}$, Tafel slope** | **Reference** |
|---|---|---|---|
| Co-$C_3N_4$/C | $V_0$ = 0.95 V<br>$n_e$ = 3.80 | $V_0$ = 1.65 V<br>Tafel = 53 mV $dec^{-1}$ | Niu *et al.*<br>*ACS Catal.*<br>2018, **8,** 1926−1931 |
| Co-$C_3N_4$/CNT | $V_0$ = 0.90 V<br>$n_e$ = N/A | $V_0$ = 1.61 V<br>Tafel = 68 mV $dec^{-1}$ | Zheng *et al.*<br>*J. Am. Chem. Soc.* 2017,<br>**139,** 3336−3339 |
| g-$C_3N_4$ /$Ti_3C_2$ nanosheets | $V_0$ = 0.80 V<br>$n_e$ = N/A | $V_0$ = 1.65 V<br>Tafel = 74 mV $dec^{-1}$ | Ma *et al.*<br>*Angew. Chem. Int. Ed.* 2016,<br>**55,** 1138-1142 |
| phosphorus-doped g-$C_3N_4$/carbon-fiber paper | $V_0$ = 0.84 V<br>$n_e$ = N/A | $V_0$ = 1.63 V<br>Tafel = 61 mV $dec^{-1}$ | Ma *et al.*<br>*Angew. Chem. Int. Ed.* 2015,<br>**54,** 4646–4650 |
| $NiCo_2S_4$@g-$C_3N_4$-CNT | $V_0$ = 0.85 V<br>$n_e$ = N/A | $V_0$ = 1.58 V<br>Tafel = 57 mV $dec^{-1}$ | Han *et al.*<br>*Adv. Mater.*<br>2019, **31,** 1808281 |
| Ag/ g-$C_3N_4$/$Co_3O_4$ | $V_0$ = 0.82 V<br>$n_e$ = 4.00 | $V_0$ = 1.65 V<br>Tafel = N/A | Guo *et al.*<br>*J. Energy Chem.*<br>2020, **41,** 185-193 |
| $Co_4N$/g-$C_3N_4$ | $V_0$ = 0.94 V<br>$n_e$ = 3.90 | $V_0$ = 1.54 V<br>Tafel = 69 mV $dec^{-1}$ | Wang *et al.*<br>*Chem. Eng. J.*<br>2021, **413,** 127954 |
| g-$C_3N_4$/NOGA | (n-type CN-NOGA)<br>$V_0$ = 0.79 V<br>$n_e$ = 3.80 | (p-type CN-NOGA)<br>$V_0$ = 1.49 V<br>Tafel = 68 mV $dec^{-1}$ | This Work |